




# Digital Image Correlation Based Internal Friction Characterization in Granular Materials

R. Venkatesh<sup>1</sup> · A. Voloshin<sup>2</sup> · I. Emri<sup>1</sup> · M. Brojan<sup>1</sup> · E. Govekar<sup>1</sup> 

Received: 9 May 2019 / Accepted: 16 December 2019  
© The Author(s) 2020

## Abstract

Based on the realization that Newtonian fluids have the unique property to redirect the forces applied to them in a perpendicular direction, a new apparatus, called the Granular Friction Analyzer (GFA), and the related GFA index, were proposed for characterizing the internal friction and related flow behavior of granular materials under uniaxial compression loading. The calculation of the GFA index is based on the integration of the internal pressure distribution along the cylinder wall, within which the granular material is being uniaxially compressed by a piston. In this paper an optical granular friction analyzer (O-GFA) is presented, where a digital image correlation (DIC) method is utilized to assess the cylinder strains used to calculate the internal pressure distribution. The main advantage of using the DIC method is that the starting point (piston–powder contact point) and the length of the integration considering the edge effects can be defined. By using the DIC full-field, instead of a few points strain measurements, a 2% improvement of the GFA index's accuracy has been achieved and its robustness with respect to the number of points has been demonstrated. Using the parametric error analysis it has been shown that most of the observed total error (7.5%) arises from the DIC-method-based measurements of the strains, which can be improved by higher-resolution cameras and DIC algorithms for the strain evaluation. Additionally, it was shown that the GFA index can be used for determining the well-known Janssen model parameters. The latter was demonstrated experimentally, by testing three SS 316 L granular material samples with different mean particle sizes. The results confirm that the mean particle size regulates the internal friction of granular materials.

**Keywords** Granular materials · Uniaxial compression · Internal friction · Flowability · Digital image correlation

## Introduction

Granular materials are defined as collections of discrete solid particles. Various examples of these materials, made from metals, ceramics and polymers, are used in many branches of industry. These include polymer and metal powders in manufacturing, sand and cement in civil engineering, grains and milk powder in the food industry, seeds and pulses in agriculture, tablets and substances in the pharmaceutical industry, and coal, minerals and ores in mining industry. All granular-material-based applications are faced with different handling processes, such as the filling, conveying,

transporting, vibrating and storing of granular materials [1–3], which are influenced by the flowability of the granular material. The ability of particles to flow is thus one of the most important properties of granular materials as it directly influences the quality and costs of manufacturing the product [2]. As an example, in powder injection-moulding technology, a too low flowability represents a serious risk in an industry that uses granular materials to manufacture critical components for the automotive, aerospace, and mould/die industries, where the density of parts and their mechanical properties are of crucial importance [4]. Another example is the pharmaceutical industry, which faces complications during the tablet-filling process, where the proper and constant flowability of granular materials plays a significant role in maintaining a uniform mass and content of the tablets [5]. Therefore, knowing an accurate value for the flowability of granular materials would enable engineers to carefully design the granular-material handling processes to avoid possible dramatic or catastrophic failures in granular-material-based industries [3].

✉ E. Govekar  
edvard.govekar@fs.uni-lj.si

<sup>1</sup> Faculty of Mechanical Engineering, University of Ljubljana, Aškerčeva cesta 6, 1000 Ljubljana, Slovenia

<sup>2</sup> Department of Mechanical Engineering and Mechanics, Lehigh University, 19 Memorial Drive West, Bethlehem, PA 18015, USA



Together with the material properties and the particle size, the flowability of a granular material is also influenced by the method of handling and the characteristics of the equipment used for the handling. In this context flowability is not an intrinsic material property of the granular material, but also depends on the handling process and the conditions under which the flow takes place [6]. In relation to this, to characterise the flowability of granular materials in general, we have to measure the internal friction that takes place within the granular material due to interparticle interactions and external particle interactions related to the handling process, the conditions and the equipment. Therefore, an experimental setup for the characterisation of a granular material's behaviour should more-or-less replicate the handling process and equipment [2]. From this point of view, many investigations have been focused on the characterisation of complex interactions [7] and a related experimental estimation of the friction in granular materials under various loading conditions, such as gravity [8–10], shear [11, 12] and uniaxial [2, 3] compressive loading.

The case of the uniaxial compression type of loading with respect to granular materials in a confined volume more-or-less replicates the real-time scenario in many real operations. One of the archetypal examples [1] is silo storage, where granular materials undergo uniaxial compressive deformation (compactification) due to gravity. Another example is tablet manufacturing, where granular materials are compressed under high pressure. However, the complex interparticle interactions and particle–wall interactions during the uniaxial compression of granular materials in a confined volume are still not well understood. Therefore, Chung et al. [3] developed a uniaxial compression experimental setup for evaluating the frictional properties of granular materials based on evaluating the stresses acting within the granular materials and on the walls of the storage container. Moreover, based on the realization that Newtonian fluids have the unique property of redirecting forces applied to them in a perpendicular direction, Bek et al. [2] independently used the same uniaxial compression approach, named the Granular Friction Analyzer (GFA), to evaluate the internal friction and the conditions under which granular materials will start to flow. For this purpose in [2], the GFA index was defined based on the ratio between the mean vertical internal pressure  $P_V$  in the granular material and the assumed hydrostatic pressure  $P_F$  of a Newtonian fluid both acting inside a cylinder along its length due to the applied uniaxial compression load. It was also shown by Schulze et al. [13] that since the GFA apparatus follows Janssen's theory and equations, it would be easier to measure the GFA index directly in an apparatus such as the GFA than to measure the individual properties of granular materials, including the internal friction and the lateral pressure ratio. The drawback of evaluating the GFA index using an uniaxial compression experimental setup [2] is related to the small number of strain-gauge-based measuring points of the cylinder wall strains

along the length of the cylinder, which were used to calculate the vertical internal pressure  $P_V$  along the cylinder length. For this reason, the stress-strain states between the measuring points were not known, which decreased the accuracy of the GFA index's estimation. Moreover, in accordance with Schulze et al, the validation of the GFA index should take place close to the piston [13], but far enough away to avoid edge effects, which might not always be possible due to the size limitations of the strain gauges.

In this paper we propose an improved GFA apparatus, which instead of strain gauges uses an optical measurement setup based on the digital image correlation (DIC) method to measure the strains along a selected length of the cylinder. In this way, the number of measuring points is significantly increased and, if necessary, the major stress-strain transformations can be captured closer to the applied compression load to increase the accuracy of the GFA index. For this purpose, a detailed description of the GFA index and the theoretical background are presented in the next section. In the third section the experimental setup and methods, including the O-GFA apparatus, determination of the GFA index calculation region, the O - GFA apparatus validation, the used materials and the performed experiments are described. In the fourth section the results of the GFA-index calculation for SS 316 L powder samples with three different mean particle sizes are presented and the defined Schulze model [13] that relates the Janssen parameters with the GFA index is experimentally confirmed. At the end of the fourth section, preceding the discussion of the results, the influences of the number of points and their proximity to the piston on the GFA-index calculation are analysed. Section five draws the conclusions.

## GFA Index

The GFA index was introduced by Bek et al. [2]. It makes it possible to characterise the internal friction  $\mu_{av}$  in granular materials and the related flowability of the uniaxially compressed granular material in a cylinder by considering the inter-particle and the particle–cylinder-wall interactions. For this purpose, as shown in Fig. 1, the behaviour of a Newtonian fluid and a granular material within a closed cylinder subjected to a uniaxial compression force  $F_T$  are considered and compared. Under a uniaxial compression force  $F_T$  in the Newtonian fluid (Fig. 1(a)) the internal hydrostatic pressure  $P_F$  is developed. The vertical internal pressure  $P_V$  and the horizontal internal pressure  $P_H$  are proportional to the constant tangential strain  $\varepsilon_t$ , whereas the constant axial strain  $\varepsilon_a$  occurs just due to the Poisson effect, as indicated in Fig. 1(a) [1, 2]. In contrast, in the case of a granular material the internal friction  $\mu_{av}$  is present. In relation to this, a difference in the vertical  $P_V(z)$  and horizontal  $P_H(z)$  internal pressures, which are decreasing along the axial direction  $z$ , can be observed [13], as

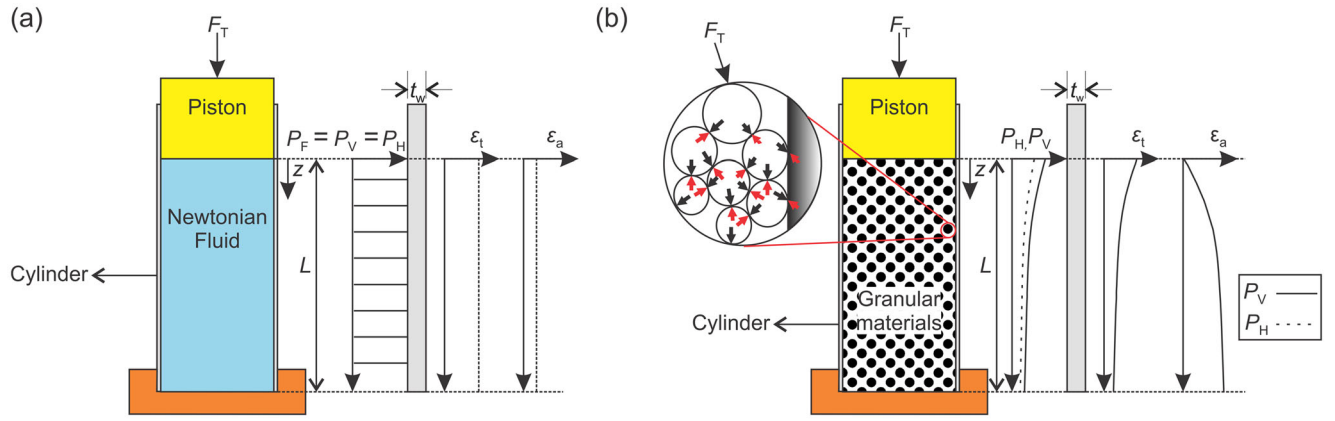


**Fig. 1** Schematics of the vertical  $P_V(z)$  and horizontal  $P_H(z)$  internal pressures, tangential  $\varepsilon_t(z)$  and axial  $\varepsilon_a(z)$  strains in the case of compressed (a) Newtonian fluid (b) granular materials

schematically indicated in Fig. 1(b). In this case the maximum of the tangential strain  $\varepsilon_t$  will be close to the piston where the force  $F_T$  is applied and will decrease in the same way as the horizontal internal pressure  $P_H$ . On the other hand, the axial strains  $\varepsilon_a$  will increase as the tangential strain  $\varepsilon_t$  decreases, because the applied force  $F_T$  is being transmitted to the cylinder walls as an axial load due to the internal friction  $\mu_{av}$  caused by the particle–wall interaction.

Based on this consideration, and according to Bek et al. [2], the dimensionless GFA index is defined as the ratio of the integral of the mean vertical internal pressure  $P_V(z)$  in the granular material along the length  $L$  of the cylinder, and the assumed theoretical pressure caused by the Newtonian fluid, under the same compression loading conditions:

$$GFA_{\text{index}} = \frac{\int_0^L P_V(z) dz}{P_F \cdot L} = \frac{A}{F_T \cdot L} \int_0^L P_V(z) dz = \frac{S_g}{S_f} \quad (1)$$

In equation (1)  $S_g$  denotes the surface area under the graph of the vertical internal pressure  $P_V(z)$  of a granular material and  $S_f$  is the surface area under the assumed theoretical constant hydrostatic internal pressure  $P_F$  of the Newtonian fluid, as shown in Fig. 2(a). The symbol  $F_T$  denotes the applied uniaxial compression force on the granular material,  $A$  is the internal area of the cylinder, and  $L$  is the integration length equal to the filling height of the granular material after the applied uniaxial force  $F_T$ . Based on the definition, the value of the GFA index is in the range between 0 and 1. Granular materials with a GFA index close to 1 behave like a fluid. If the GFA index decreases, it indicates the amplification of the internal friction  $\mu_{av}$  and the decreased flowability of the granular material. Since the vertical internal pressure  $P_V(z)$  is a monotonically decreasing function, we can evaluate the internal friction  $\mu_{av}$  properties of granular materials and the related GFA index by analysing the decrease of vertical internal pressure  $P_V$  along the length  $L$  of the cylinder. Granular materials with a rapid decrease of the vertical internal pressure  $P_V$  have a lower GFA index and higher internal friction  $\mu_{av}$  than the

materials with a lower decrease of the vertical internal pressure  $P_V$ .

In order to determine the GFA index experimentally, the interrelation between the vertical internal pressure  $P_V$  and the corresponding strains generated at the outer surface of the cylinder [3], defined by:

$$P_V = \frac{4 \cdot F_V}{\pi D_i^2 \cdot (1 + \varepsilon_t)^2}, \quad (2)$$

is needed. In the above equation, the unknown vertical internal force  $F_V$  can be calculated by considering the free-body diagram shown in Fig. 2(b), as follows:

$$F_V = F_T + \pi D_i \cdot (1 + \varepsilon_t) \cdot t_w \cdot \sigma_a \quad (3)$$

The unknown axial stress  $\sigma_a$  on the cylinder wall in equation (4) can be calculated [14] using the following expression:

$$\sigma_a = \frac{E_w (\varepsilon_a + \nu_w \cdot \varepsilon_t)}{1 - \nu_w^2} \quad (4)$$

Here,  $E_w$  and  $\nu_w$  denote the Young's modulus and the Poisson's ratio of the cylinder wall, whereas  $\varepsilon_t$  and  $\varepsilon_a$  denote the tangential and axial strains of the cylinder wall. Taking the measurements of the tangential  $\varepsilon_t$  and the axial  $\varepsilon_a$  strain on the cylinder wall at  $n$  points along the  $z$  axis, the related vertical internal pressure  $P_V(z)$  can be calculated using equations (2), (3) and (4). Knowing  $P_V(z)$ , the related surface area  $S_g$  can be computed with a numerical integration. Based on this, it is evident that the accuracy of the calculated surface area  $S_g$  and the related GFA index are affected by the number of  $n$  measurement points.

By considering the case of a confined compression of granular materials, also the parameters of the Janssen model [8], including the internal pressure ratio  $K_{av}$  and internal friction coefficient  $\mu_{av}$ , can be evaluated. The internal pressure ratio  $K_{av}$  is defined as the ratio of the horizontal  $P_H$  to the vertical  $P_V$  internal pressure:

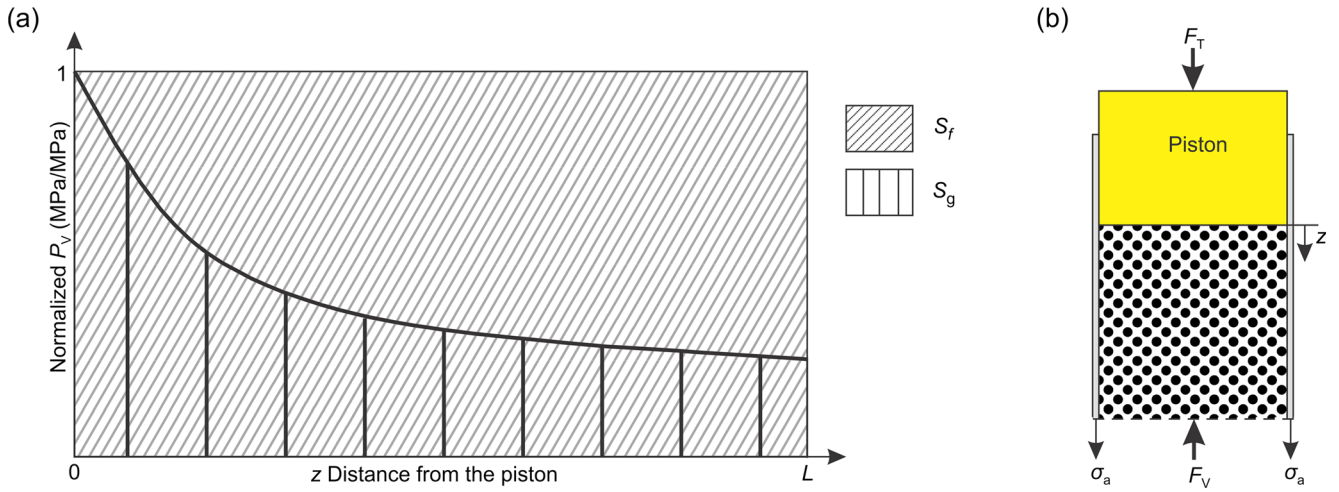


Fig. 2 (a) Schematic graphical definition of GFA index. (b) Free-body diagram of the piston, cylinder and granular material assembly

$$K_{av} = \frac{P_H}{P_V} \quad (5)$$

Here, the horizontal internal pressure  $P_H$  is calculated based on the thin-walled-pressure-vessel theory:

$$P_H = \frac{(D_o - D_i) \cdot \sigma_t}{D_i \cdot (1 + \varepsilon_t)} \quad (6)$$

where  $D_o$  and  $D_i$  denote the outer and inner diameters of the cylinder, and  $\sigma_t$  and  $\varepsilon_t$  the tangential stress and strain on the cylinder wall, respectively. The tangential stress  $\sigma_t$  on the cylinder wall is calculated based on the plane stress equation:

$$\sigma_t = \frac{E_w(\varepsilon_t + \nu_w \cdot \varepsilon_a)}{1 - \nu_w^2} \quad (7)$$

The second Janssen parameter, the internal friction coefficient  $\mu_{av}$ , is defined as the ratio of shear stress  $\tau_w$  and the horizontal internal pressure  $P_H$ :

$$\mu_{av} = \frac{\tau_w}{P_H} \quad (8)$$

Since the shear stress  $\tau_w$  is not known we cannot evaluate the internal friction coefficient  $\mu_{av}$  exerted by the granular material on the cylinder wall, using equation (8). However, using the calculated values of the vertical internal pressure  $P_V(z)$  and Janssen's simplified vertical internal pressure  $P_V$  equation [13]:

$$P_V(z) = \sigma_{v0} \cdot e^{-4 \cdot K_{av} \cdot \mu_{av} \cdot \frac{z}{D_i}} \quad (9)$$

where  $\sigma_{v0}$  denotes the applied vertical stress on the top of the granular materials and  $z$  denotes the vertical coordinate along the length  $L$  of the cylinder, the internal friction coefficient  $\mu_{av}$  can be evaluated using the exponential regression method.

Furthermore, based on the known Janssen parameters  $K_{av}$  and  $\mu_{av}$ , and taking into account the vertical internal pressure  $P_V$  instead of the horizontal  $P_H$ , by using the procedure described in [13], the GFA index can be defined by:

$$GFA_{index} = \frac{D_i}{4 \cdot K_{av} \cdot L \cdot \mu_{av}} \cdot \left[ 1 - e^{-\frac{4 \cdot K_{av} \cdot \mu_{av} \cdot L}{D_i}} \right] \quad (10)$$

It is evident from equation (10) that the GFA index, in addition to the internal pressure ratio  $K_{av}$  and the internal friction coefficient  $\mu_{av}$ , also depends on the  $D_i/L$  ratio of the cylinder.

## Experimental Setup and Methods

### O-GFA apparatus and DIC method

As described above, to evaluate the GFA index experimentally the tangential  $\varepsilon_t$  and axial  $\varepsilon_a$  strains along the axial direction  $z$  of a cylinder filled with a granular material and uniaxially compressed should be measured. For this purpose, a GFA apparatus was designed [2], which consists of a closed-bottom stainless-steel cylinder and a stainless-steel piston, as shown in Fig. 3(a). The stainless-steel piston is used to apply the uniaxial compression force  $F_T$  to the granular material contained in the cylinder. Due to the applied compression force  $F_T$  on the granular materials, the vertical  $P_V$  and horizontal  $P_H$  internal pressures are developed, and the cylinder undergoes deformations in the tangential and axial directions. To measure these deformations, Bek et al. [2] proposed an apparatus based on strain-gauge measurements at three different points along the axial direction  $z$  of the cylinder, as shown in Fig. 3(a). The major drawback of this method is the ability to measure strains at only a few points, and the fact that the vertical internal pressure  $P_V$  between the strain gauges and the changes of the vertical internal pressure  $P_V$  close to the piston

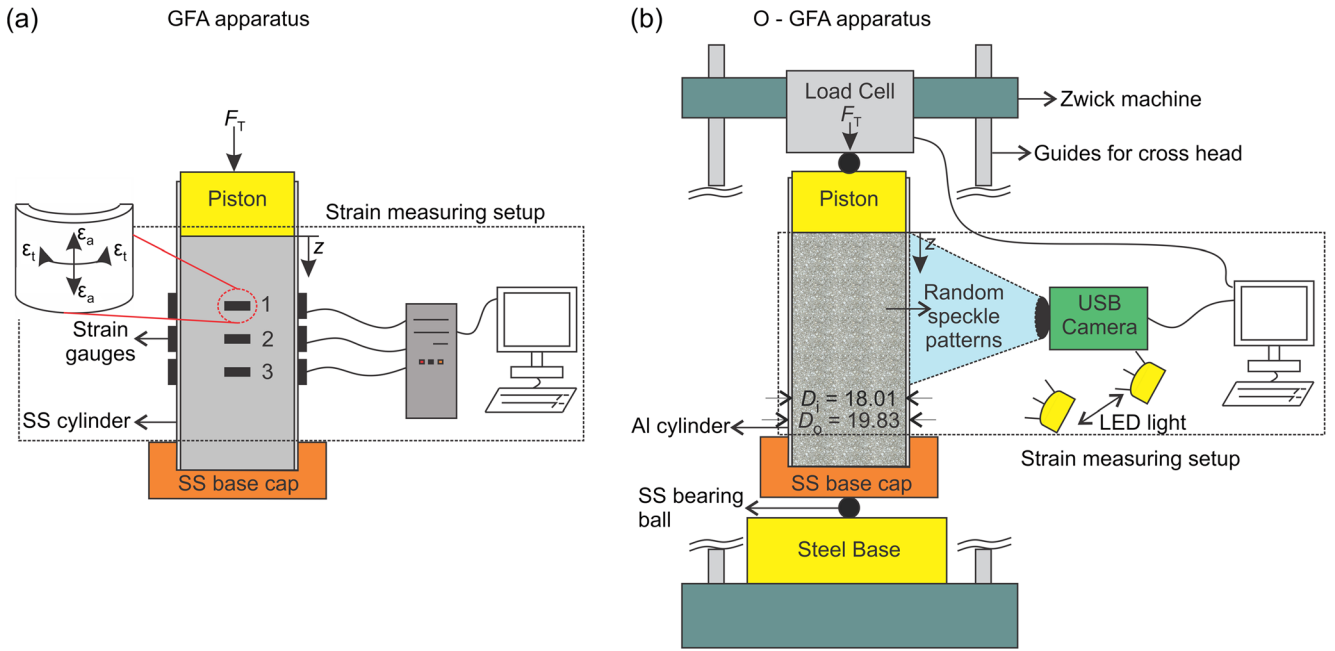


**Fig. 3** Schematics of: (a) the strain-gauge-based GFA apparatus and (b) the DIC-based O-GFA apparatus

cannot be captured due to the strain gauge's dimensions and the lack of the space, which all affect the accuracy of the GFA index calculation.

To eliminate these drawbacks and to improve the accuracy of the GFA index calculation, a new optical granular friction analyser (O-GFA) was designed, as schematically presented in Fig. 3(b). It consists of an aluminium cylinder of outer diameter  $D_o = 19.83$  mm, a stainless-steel piston, a digital monochromatic USB 3.1 camera of 5 MP, and two LED illumination sources. To ensure higher strains caused by the uniaxial compression of the granular material contained inside of the aluminium cylinder, a thin-walled cylinder of thickness 0.91 mm was selected. Additionally, the inner surface of the aluminium cylinder was polished to decrease the friction between the powder grains and the inner surface of the cylinder, and the potential indentation of the grains into the surface.

Similarly, as in the case of using the GFA apparatus, the Zwick Z050 universal testing machine was used to apply a uniaxial compression force  $F_T$  in a controlled manner to the piston. To ensure symmetrical uniaxial loading, the loading force was applied in the axis of the piston and the cylinder through the SS bearing balls which were placed between the load cell and the piston, and between the SS base cap and steel base, as shown schematically in Fig. 3(b). A digital camera was used to capture digital images of random speckle patterns applied to the cylinder in the DIC region used for the measurement of the tangential  $\varepsilon_t$  and axial  $\varepsilon_a$ , strains. For this purpose, digital images of random speckle patterns before and after the achieved pre-set uniaxial compression loading  $F_T$  of the sample were taken. Using the DIC method, the random speckle patterns of the two digital images [15] are

compared using an image-correlation-and-processing algorithm Ncorr [16] to determine the deformation and related tangential  $\varepsilon_t$  and axial  $\varepsilon_a$  strains fields [17]. In the Ncorr algorithm the parameters used for the DIC were: subset size  $25 \times 25$  pixels, spacing 3 pix, iteration resolution 1e-006, and number of iterations 50. Examples of a contour plot of the tangential  $\varepsilon_t$  and axial  $\varepsilon_a$  strain field obtained by the DIC method, represented by 25 points along the width  $w$  and 270 points along the  $z$  axis, are shown in Fig. 4.

### Determination of the GFA index calculation region

In accordance with equation (1), the GFA index depends, in addition to the vertical internal pressure  $P_V(z)$  calculated from the measured average strains  $\bar{\varepsilon}_t(z)$  and  $\bar{\varepsilon}_a(z)$ , on the integration length  $L$  along the  $z$  axis, starting at the piston-powder contact point. Theoretically, as defined in Section 2, the integration length  $L$  is equal to the height of the granular material contained in the cylinder. However, in the experiment the average strains  $\bar{\varepsilon}_t$  and  $\bar{\varepsilon}_a$ , along the length  $L$  are influenced by several factors that should be considered to ensure accurate and repeatable measurements of the strain. At the top of the cylinder the strains are affected by the edge effect due to the piston, and at the bottom by the DIC method based strain measurement resolution due to the decrease of the tangential  $\varepsilon_t$  strains along the length of the cylinder and by the edge effect due to the base cap. Therefore, the piston-powder contact point, the proper integration length  $L$ , considering the DIC method's strain measurement resolution, and the boundary of the edge affected regions at the top and bottom of the cylinder

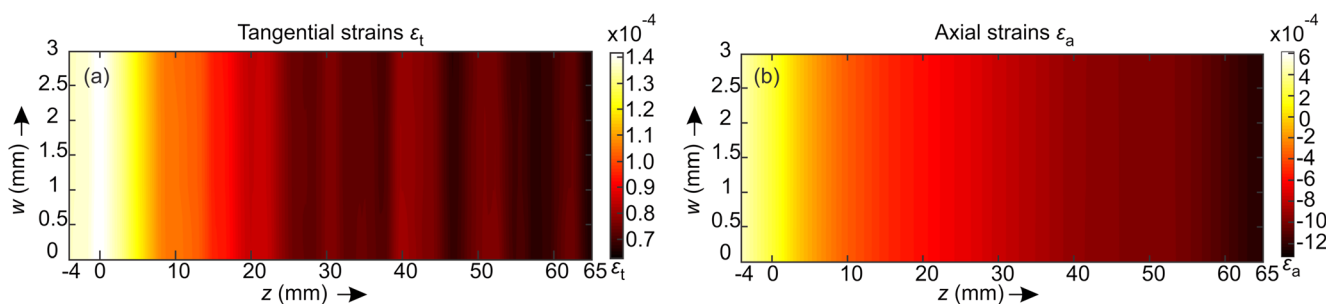


**Fig. 4** Examples of contour plot of (a) tangential  $\varepsilon_t$  and (b) axial  $\varepsilon_a$  strain fields of width  $w = 3$  mm along the axial direction  $z$  of the aluminium cylinder

defining the GFA index calculation region should be determined accordingly.

For this purpose, based on a seven average of the tangential  $\varepsilon_t(z)$  and axial  $\varepsilon_a(z)$  strains calculated over the 25 points along the 3 mm width  $w$  of the contour plot of the strain fields, the average tangential  $\bar{\varepsilon}_t(z)$  and axial  $\bar{\varepsilon}_a(z)$  strains and the related vertical internal pressure  $P_V(z)$  have been calculated. In Fig. 5 an example of graphs of average tangential  $\bar{\varepsilon}_t(z)$  strain and vertical internal pressure  $P_V(z)$ , calculated for the case of the powder of mean particle size  $m = 105 \mu\text{m}$ , are shown. In the average tangential strain  $\bar{\varepsilon}_t(z)$  signal shown in Fig. 5(a) a peak value can be observed. The peak value corresponds to the piston-powder contact point defining the origin  $z = 0$ , i.e., the starting point of the integration length  $L$  in the calculation of the GFA index along the  $z$  axis. Based on the DIC method's strain measurement resolution the integration length  $L = 65$  mm was selected to ensure the tangential  $\varepsilon_t$  strains are above  $400 \mu\epsilon$ . Furthermore, a pressure  $P_V(z)$  higher than the applied stress  $\sigma_{v,0} = 19.02$  MPa, can be observed in the region close to the piston (Fig. 5(b)). Using the criterion  $P_V(z) > \sigma_{v,0}$ , the distance  $z_{\text{ef}} = 18$  mm from the piston was defined as the boundary of the edge effect due to the piston. Based on the presented consideration, the upper and bottom boundaries of the speckle pattern region used for the DIC method based calculation of the GFA index were selected to be 18 mm and 65 mm below the piston-powder contact point. Further, by taking into account the design of the O-GFA apparatus, the bottom boundary of the speckle pattern and the related GFA

index calculation region was 90 mm above the bottom base cap (Fig. 6), which ensures that the captured speckle pattern is not affected by the edge effect due to the bottom base cap.

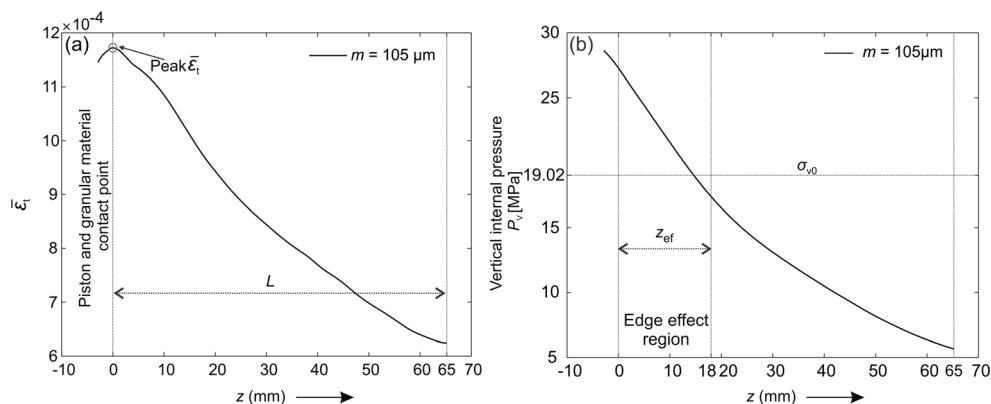
A digital image of the speckle pattern of width  $w = 3.0$  mm and height  $h = 47.0$  mm composed of  $75 \times 690$  pixels was used in the DIC-method-based calculation of the strains  $\varepsilon_t$  and  $\varepsilon_a$ , related internal pressure  $P_V(z)$  and the GFA index.

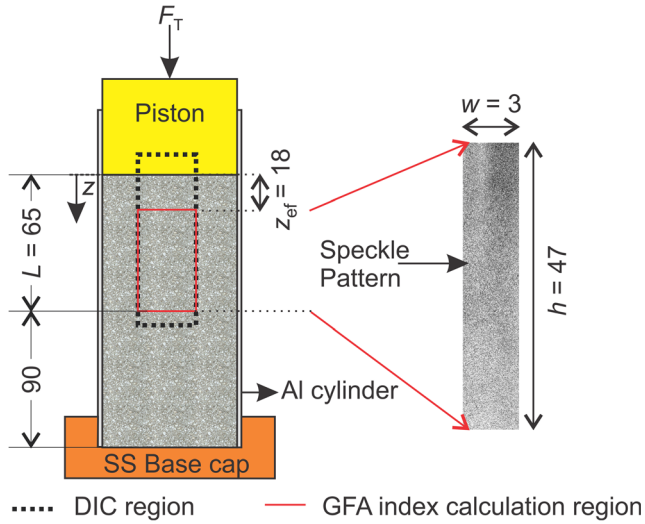
### Validation of the O-GFA apparatus

The calculation of the GFA index using the O-GFA apparatus is based on a DIC measurement of the tangential  $\varepsilon_t$  and axial  $\varepsilon_a$  strains. Therefore, the accuracy of the strain measurements is of primary importance. To validate the DIC method's strain-measurement accuracy, the strains of an empty cylinder loaded with a uniaxial compression force  $F_T$ , obtained experimentally by the O-GFA apparatus, were compared to the strains calculated from the analytical model of an empty aluminum cylinder exposed to a known uniaxial compression force  $F_T$ .

To validate the measurements of tangential  $\varepsilon_t$  and axial  $\varepsilon_a$  strains measurements using the DIC method, the empty aluminium cylinder was loaded five times at each of the pre-set compression forces  $F_T = 3010$  N, 4510 N and 4910 N using the Zwick machine and related mean tangential  $\varepsilon_t$  and axial  $\varepsilon_a$  strains over the GFA index calculation region were calculated. Additionally, for the experimental evaluation of the axial stress  $\sigma_a$  of the cylinder wall and for the purpose of analytically modelling, the mean strains, the mean values and related

**Fig. 5** (a) Example of the mean value of a tangential strain  $\bar{\varepsilon}_t(z)$  and determination of the piston-powder contact i.e. starting point of the integration in calculation of the GFA index for the mean powder particle size  $m = 105 \mu\text{m}$ , (b) Example of the vertical internal pressure  $P_V(z)$  and the determination of the edge-effected region due to the piston at the top of the cylinder





..... DIC region      — GFA index calculation region  
**Fig. 6** Position of the DIC region and DIC method based GFA index calculation region. All dimensions are in mm

standard deviations of the inner  $D_i = 18.01 \pm 0.01$  mm, and outer  $D_o = 19.83 \pm 0.01$  mm diameters of the aluminium cylinder were calculated based on the 30 measurements with a digital calliper.

In Fig. 7(a) a scatter plot of experimental mean axial strain  $\varepsilon_a$  of the aluminium cylinder denoted by square vs. theoretical axial strain  $\varepsilon_{at}$  calculated using the Young's modulus  $E_w = 69.5$  GPa [18] of the aluminium material is shown. The related regression coefficient  $r = 0.98$ , and the experimentally evaluated Young's modulus  $E_w = 69.0 \pm 3.2$  GPa, which deviates by less than 1% from the theoretical value, indicate a high accuracy of the measured axial strain  $\varepsilon_a$ . Similarly, in Fig. 7(b), the experimental values of the tangential strain  $\varepsilon_t$  vs the theoretical tangential strain  $\varepsilon_{tt}$  calculated by considering the Poisson's ratio  $\nu_w = 0.33$  [19] of aluminium are shown. The calculated regression coefficient  $r = 0.84$  and the experimentally evaluated Poisson's ratio  $\nu_w = 0.34 \pm 0.03$ , deviates by 2.9% from the theoretical value, which indicates a slightly

lower accuracy of the tangential strain  $\varepsilon_t$  measurements. Low accuracy of the measured tangential strains  $\varepsilon_t$  could be related to the relatively low resolution of the camera and to the curvature of the cylinder that has not been taken into account by the planar image of the digital camera.

In addition to the measurement accuracy of the strains, the calculation of the GFA index is influenced by the uncertainty of the calculated vertical internal pressure  $P_V$  from the measured tangential  $\varepsilon_t$  and axial  $\varepsilon_a$  strains. For the purpose of a comparison of the results reported in [2], the uncertainty of the vertical internal pressure  $P_V$  was evaluated using a parametric error-analysis method [2, 20]. By substituting equation (4) into (3) and (3) into (2) and implementing the parametric error-analysis method, the uncertainty of the vertical internal pressure  $\Delta P_V$  is given by:

$$\begin{aligned} \Delta P_V \cong & \left| \frac{\partial P_V}{\partial D_o} \Delta D_o \right| + \left| \frac{\partial P_V}{\partial D_i} \Delta D_i \right| + \left| \frac{\partial P_V}{\partial E_w} \Delta E_w \right| \\ & + \left| \frac{\partial P_V}{\partial \nu_w} \Delta \nu_w \right| + \left| \frac{\partial P_V}{\partial \varepsilon_t} \Delta \varepsilon_t \right| + \left| \frac{\partial P_V}{\partial \varepsilon_a} \Delta \varepsilon_a \right| \\ & + \left| \frac{\partial P_V}{\partial F_t} \Delta F_t \right| \end{aligned} \quad (11)$$

where  $\Delta$  denotes the standard deviation of a particular parameter. To estimate the standard deviations that take place together with the partial derivate of each variable, in addition to geometrical measurements of the cylinder diameters  $D_o$  and  $D_i$ , five trials of the measured tangential  $\varepsilon_t$  and axial  $\varepsilon_a$  strains at the compression load  $F_T = 4510$  N were considered. The calculated error contributions of each of the variables are shown in Table 1. It can be seen that the relative error in the measured pressure  $\Delta P_V / P_V$  is approximately 7.54%, which is lower than reported in [2]. Similarly, the highest contribution to the error arises from the Young's modulus  $E_w$  (33.8%) and the Poisson's ratio  $\nu_w$  (28.6%), followed by the axial strains  $\varepsilon_a$  (23.3%), and the tangential strain  $\varepsilon_t$  (5.28%), while the total

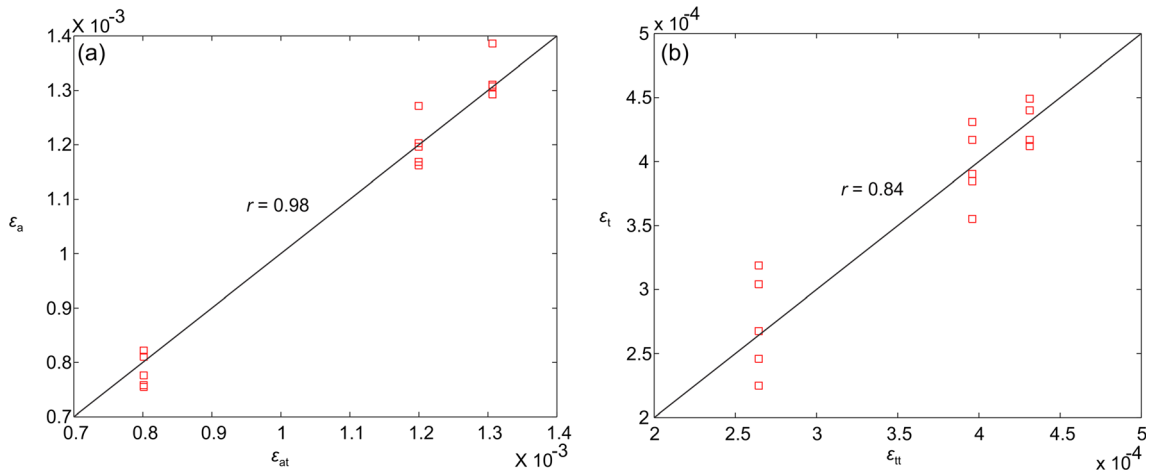


**Fig. 7** Scatter plots: (a) Measured  $\varepsilon_a$  vs. theoretical  $\varepsilon_{at}$  axial strains (b) Measured  $\varepsilon_t$  vs. theoretical tangential  $\varepsilon_{tt}$  strains

**Table 1** Contribution of the individual terms to the total relative pressure

Parameter	$\left  \frac{\partial P_V}{\partial D_o} \Delta D_o \right $	$\left  \frac{\partial P_V}{\partial D_i} \Delta D_i \right $	$\left  \frac{\partial P_V}{\partial E_w} \Delta E_w \right $	$\left  \frac{\partial P_V}{\partial \nu_w} \Delta \nu_w \right $	$\left  \frac{\partial P_V}{\partial \varepsilon_t} \Delta \varepsilon_t \right $	$\left  \frac{\partial P_V}{\partial \varepsilon_a} \Delta \varepsilon_a \right $	$\left  \frac{\partial P_V}{\partial F_t} \Delta F_t \right $	Total
$\Delta$	0.01 mm	0.01 mm	3.2 GPa	0.03	29 E-6	43 E-6	38 E-6	/
$\frac{\Delta P_V}{P_V}$ in%	0.3	0.38	2.55	2.16	0.39	1.76	0.001	7.54
Contribution of error to total error in %	3.96	5.03	33.9	28.58	5.28	23.28	0.0001	100

error arising from the cylinder geometry and the force sensor is (9.03%).

Since the Poisson's ratio  $\nu_w$  and Young's modulus  $E_w$  are related to the tangential  $\varepsilon_t$  and axial  $\varepsilon_a$  strains we can conclude from the results of the parametric error analysis that the uncertainty of the vertical internal pressure  $P_V$  can be decreased by a decrease in the measurement uncertainty of the tangential  $\varepsilon_t$  and axial  $\varepsilon_a$  strains. In our case this can be done by using a camera with a higher resolution and a cylinder with lower  $E_w$ .

## Materials and experiments

For the purpose of the performance demonstration for the O-GFA apparatus, the GFA index of three samples of stainless-steel 316 L granular material with different mean particle size values  $m = 69 \mu\text{m}$ ,  $105 \mu\text{m}$  and  $130 \mu\text{m}$  and related standard deviations  $\Delta$  reported in Table 2 were considered. The related particle size distributions obtained with an image analysis of the particles are shown in Fig. 8.

For each sample of granular material, seven repetitions of the experiment were performed. Although the plastic deformation of the grains was not observed with a visual inspection using a microscope, with the aim to avoid the potential influence of the plastic deformation of the grains on the compression-load experiments, for each repetition of the experiment the cylinder was filled with a sample of unused granular material to the same level and tapped without pre-consolidation. The level was confirmed by checking the cross-head starting position of the Zwick universal testing machine. At zero load the reference image of the speckle patterns on the surface of the cylinder filled with the granular material was taken. After this, a uniaxial compression force  $F_T = 4510 \text{ N}$  was applied to the granular material through the piston and an image of the speckle pattern of the deformed cylinder was taken. During the short period of the image's acquisition, no time dependent changes related to the presence of the creep were observed. The acquired images of the speckle patterns of the unloaded and loaded cylinders were then analysed using

**Table 2** Sample mean particle size ( $\mu\text{m}$ ) and its related standard deviation

Mean particle size $m$ ( $\mu\text{m}$ )	69	105	130
Standard deviation $\Delta$ ( $\mu\text{m}$ )	6.6	7.6	14

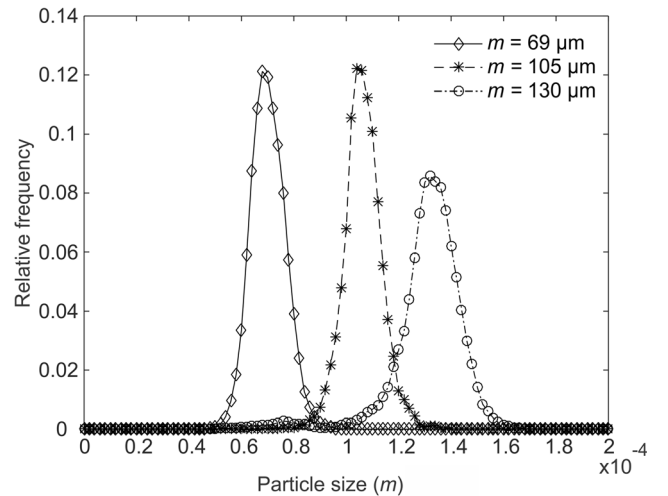
the DIC method to calculate the tangential  $\varepsilon_t$  and axial  $\varepsilon_a$  strains required for internal vertical pressure  $P_V$  and related GFA index calculation.

## Results and Discussion

### Calculation of GFA index

In Fig. 9(a) and (b) the mean values  $\bar{\varepsilon}_t(z)$  and  $\bar{\varepsilon}_a(z)$  of the measured tangential and axial strains vs. the vertical position  $z > z_{\text{ef}}$  along the cylinder for each of the different particle mean sizes  $m = 69 \mu\text{m}$ ,  $105 \mu\text{m}$  and  $130 \mu\text{m}$  are shown. The mean values  $\bar{\varepsilon}_t(z)$  and  $\bar{\varepsilon}_a(z)$  were calculated based on seven repetitions of the measurements of the tangential  $\varepsilon_t$  and axial  $\varepsilon_a$  strain fields taken within the defined GFA index calculation region, as shown in Fig. 6.

From Fig. 9 it is evident that the positive tangential strains  $\bar{\varepsilon}_t$  (Fig. 9(a)) decrease and the negative axial strains  $\bar{\varepsilon}_a$  (Fig. 9(b)) increase along the axial  $z$  direction of the cylinder. The observed dependencies of the tangential  $\bar{\varepsilon}_t$  and axial  $\bar{\varepsilon}_a$  strains on the vertical position  $z$  are due to the internal interparticle and particle-wall friction  $\mu_{\text{av}}$ . Based on the tangential  $\bar{\varepsilon}_t$  and axial  $\bar{\varepsilon}_a$  strains, the vertical  $P_V$  and the horizontal  $P_H$  internal pressures acting inside the cylinder along the  $z$  axis at the

**Fig. 8** Considered sample particle size distributions with three different mean values



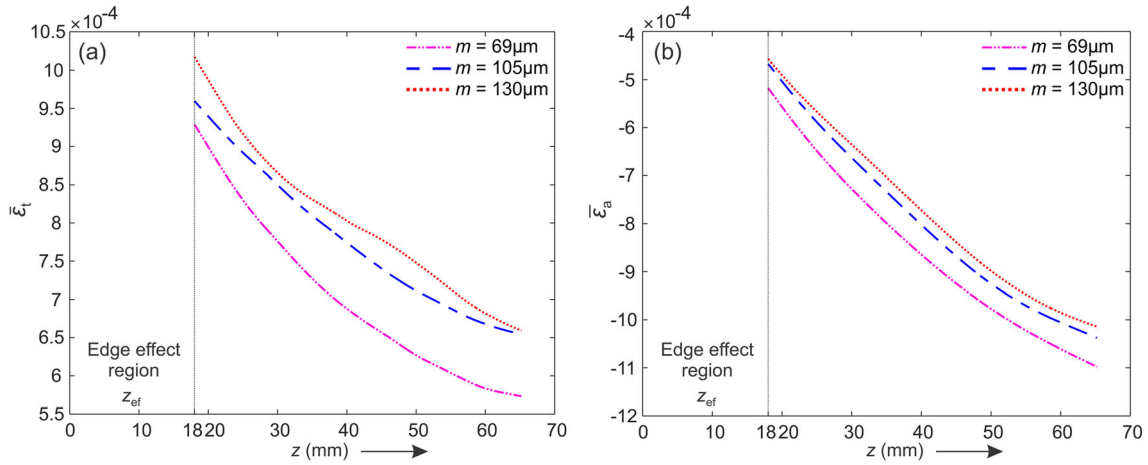


Fig. 9 Mean values of the strains vs. position  $z$  for different mean particle sizes  $m = 69, 105$  and  $130 \mu\text{m}$ . (a) tangential  $\bar{\epsilon}_t(z)$  and (b) axial  $\bar{\epsilon}_a(z)$  strain

vertical position  $z > z_{ef}$  were calculated using equations (2) and (6).

Figure 10 shows the normalized calculated values of  $P_V(z)$  and  $P_H(z)$ , using the applied vertical stress  $\sigma_{v0} = 19.02 \text{ MPa}$  corresponding to the uniaxial compression load  $F_T = 4510 \text{ N}$ . Similarly, and for the same reason as in the case of the strains, the vertical  $P_V(z)$  and horizontal  $P_H(z)$  internal pressures are decreasing with the coordinate  $z$ . Additionally, it is also evident from Fig. 10 that the pressures  $P_V(z)$  and  $P_H(z)$  decrease with the decrease of the mean size of the particle. As reported in [1, 2], this effect occurs because the smaller particles exhibit more cohesion and related increases of the internal friction  $\mu_{av}$ . The above-presented results of the dependence of the strains  $\bar{\epsilon}_t$  and  $\bar{\epsilon}_a$ , and the internal pressures  $P_H$  and  $P_V$  on the coordinate  $z$  along the cylinder below the piston as well as the observed influence of the mean particle size on the internal pressure are in agreement with the results presented in [2, 3, 13].

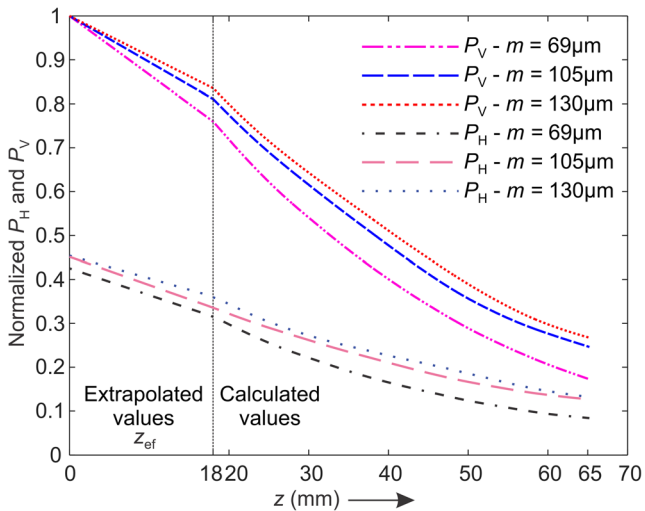
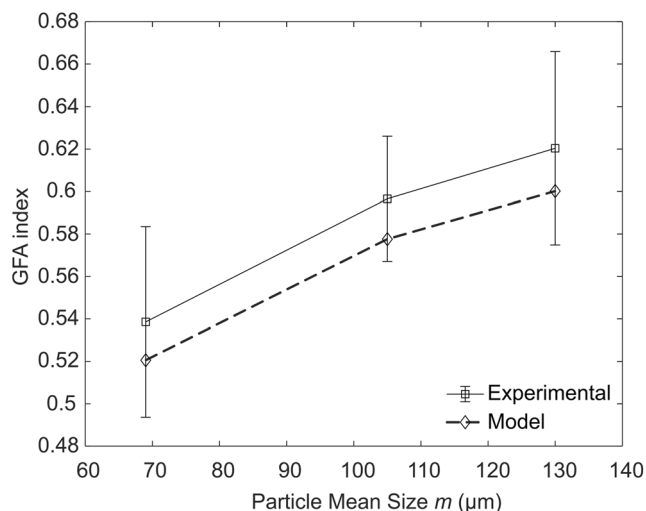


Fig. 10 Calculated and extrapolated mean values of the normalized vertical  $P_V$  and horizontal  $P_H$  internal pressures vs. the vertical position  $z$

However, to calculate the GFA index using the definition, the values of the vertical internal pressure  $P_V$  in the interval  $[0, z_{ef}]$  are also needed. Because the applied vertical stress  $\sigma_{v0}$  on the granular materials is known, the vertical internal pressure  $P_V$  at the contact point of the piston and the granular material is equal to the applied vertical stress  $\sigma_{v0}$ , and the related normalised vertical internal pressure  $P_V$  is 1. Therefore, to describe the vertical internal pressure  $P_V$  in the interval  $[0, z_{ef}]$ , the vertical internal pressure  $P_V(z = z_{ef})$  can be linearly extrapolated to 1, as shown in Fig. 10. On the other hand, as reported in [3, 13], due to internal friction  $\mu_{av}$  between the piston and the granular material during the compression loading, the horizontal internal pressure  $P_H$  close to the piston is not equal to the applied vertical internal pressure  $P_V$ . Therefore, to define the extrapolation value of the horizontal internal pressure  $P_H$  at the piston, as shown in Fig. 10, first the internal pressure ratio  $K_{av} = P_H/P_V$  was calculated and averaged along the 230 points of the GFA index calculation region (Fig. 6) for each considered powder. Knowing  $K_{av}$ , the horizontal internal pressure  $P_H$  at the extrapolated point at the contact with the piston is then given by  $P_H = K_{av} P_V$ .

Based on the vertical internal pressure values  $P_V(z)$  calculated in the interval  $[0, L]$  for each of the three granular material samples with different mean particle sizes  $m = 69 \mu\text{m}, 105 \mu\text{m}$  and  $130 \mu\text{m}$  of the particles, the GFA index was calculated using equation (1) for each of the seven repetitions of the experiment. In Fig. 11 the GFA index's mean values with the related 95% confidence intervals vs. the mean particle size  $m$  are shown as a solid line. The observed increase in the GFA index is in agreement with the results reported in [2] and has also been statistically confirmed by an ANOVA test. The calculated  $p$  value of 0.007 of the ANOVA test performed on the GFA index's mean values from seven repetitions statistically confirms the significant differences of the GFA index mean values and the related strains  $\bar{\epsilon}_t$  and  $\bar{\epsilon}_a$ , and the internal pressures  $P_V$  and  $P_H$ , used to evaluate the GFA index.



**Fig. 11** Experimental evaluation of the GFA index with 95% confidence intervals vs. the particle mean size  $m$  and a comparison with the Schulze-model-based calculation of the GFA index

Along with the GFA index evaluation, based on the analytical model developed by Schulze [13], the relation between the GFA index and Janssen's parameters, including the internal pressure ratio  $K_{av}$  and the internal friction  $\mu_{av}$  (equation (10)), was also verified. For this purpose, using equations (5) and (9), the internal pressure ratio  $K_{av}$  and the internal friction coefficient  $\mu_{av}$  for the three considered granular materials were calculated based on the experimentally obtained data. Taking into account that  $K_{av}$  does not change along the axial  $z$  of the cylinder [13] a mean value of  $K_{av}$  along the entire GFA index calculation region was calculated. Furthermore, using the mean value of  $K_{av}$ , from equation (9), the internal friction coefficient  $\mu_{av}$  was calculated. In Fig. 12 the dependence of  $K_{av}$  and the related mean value of the internal friction coefficient  $\mu_{av}$  vs. the particle mean size  $m$  are shown. It is clear that  $K_{av}$  and the internal friction coefficient  $\mu_{av}$  show similar, nonlinearly increasing and decreasing trends vs. the particle size means, as reported in [1].

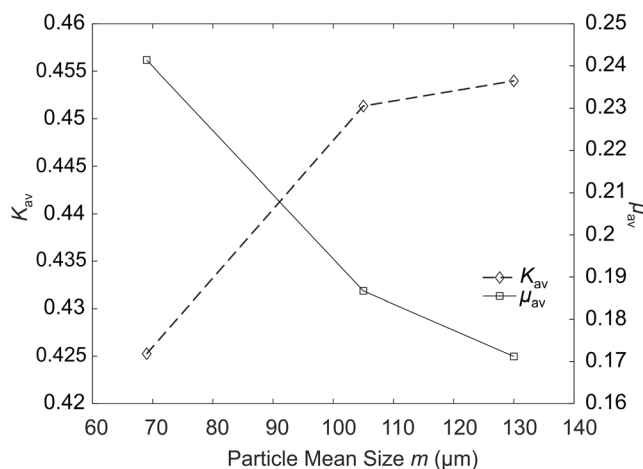


**Fig. 12** Influence of the mean particle size  $m$  on the internal pressure ratio  $K_{av}$  and the internal friction  $\mu_{av}$

Based on the calculated internal pressure ratio  $K_{av}$  and internal friction  $\mu_{av}$  the GFA index was calculated using the relation described by equation (10) and compared with the experimental result, as shown in Fig. 11. It is clear that the GFA index (solid line) calculated from the experiments and the model (dashed line) are well correlated.

### Influence of the number of points on the GFA index

When using a strain-gauge-based evaluation of the GFA index [2] the number of measurement points as well as a consideration of the granular material's behavior close to the piston are limited. In contrast, the O-GFA apparatus makes it possible to consider a larger number of points that can be located close to the piston. In Fig. 13(a) the GFA index of granular material with a mean particle size of 69  $\mu\text{m}$  vs. the number of measurement points in the range from 3 to 230 of vertical internal pressure  $P_v$  curve along the length  $L = 65$  mm obtained by the O-GFA apparatus is shown. It is clear that having fewer points the GFA index value increases exponentially after a certain threshold value of points considered in the length  $L$  and that a 2% difference in the GFA index is observed when comparing the GFA index using 3 and 230 points.

Additionally, the influence of the distance  $z_{ef}$  of the first measured point with respect to the piston on the GFA index was evaluated. In Fig. 13(b) the GFA index values, related to the relative distance  $z_{ef}/L$  of the first measured point with respect to the piston, are shown. The closest distance to the piston,  $z_{ef} = 18$  mm, was used, which reduces the influence of the cylinder's edge effect on the measurement. The graph shows a nonlinear dependence of the GFA index on the distance  $z$ . The maximum difference in the GFA index value of 1.29% was found to be at a 44.6% distance of the total length  $L$ . From the above analysis we can see that the GFA index is relatively robust with respect to both the number of points and the proximity of the first measured point to the piston is influencing the value of the calculated GFA index.

### Discussion

The presented O-GFA apparatus using the DIC method and the concept of the GFA index are shown to be a relatively simple approach to analyze and characterize the internal friction and the related flowability of the granular materials exposed to uniaxial compression loading. As stated by the Schulze et al. [13], the GFA index alone might be used to characterize the flowability of a granular material instead of measuring the individual properties of granular materials, including the internal friction and the lateral pressure ratio. One of the main expected benefits of the O-GFA apparatus was an increased number of points and their closeness to the piston used in the GFA index calculation considering the edge

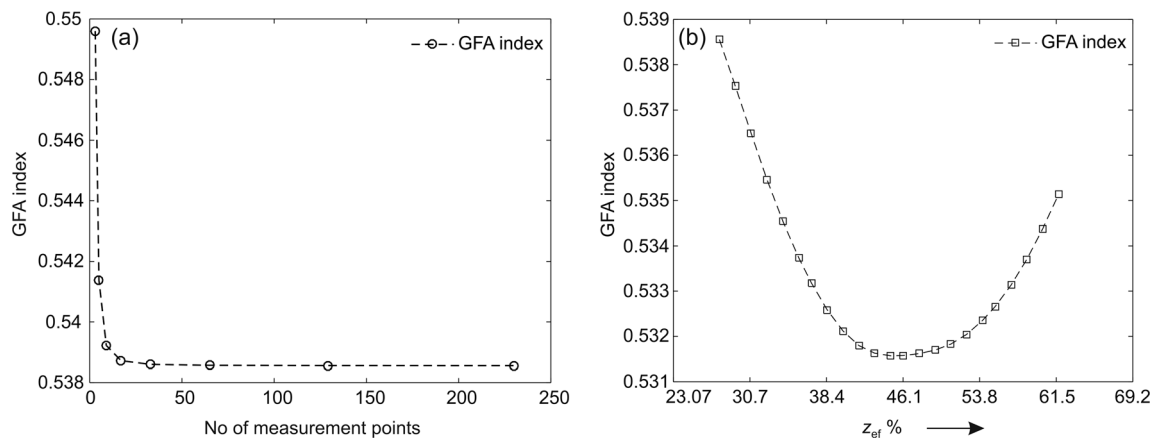


**Fig. 13** GFA index vs. (a) number of points, (b) the distance  $z = z_{ef}$  of the first measured point

effects, which brought 2.0% and 1.3% improvements in the GFA index accuracy. However, experimental results show that there are open issues, including the standardization of the integration length, and the granular material particle and cylinder diameter ratio, which should be further considered to increase the accuracy, precision of the O-GFA apparatus and the physical interpretation of the GFA index.

From the parametric error analysis of the vertical internal pressure  $P_V$ , it can be seen that most of the error in the GFA index calculation arises from the DIC-method-based measurements of the tangential  $\varepsilon_t$  and axial  $\varepsilon_a$  strains of the cylinder wall. This is related to the relatively low strain resolution provided by the current digital camera and the DIC method when compared to strain gauges and fiber optic strain gauges, which have resolutions of 1 and 0.1 micro strain, respectively. Therefore, to improve the accuracy of the calculated vertical internal pressure  $P_V$  and the related GFA index a higher-resolution camera should be used to acquire the image of the speckle pattern. Furthermore, since the DIC method depends on the speckle pattern's contrast, the speckle size, the lighting on the surface of the specimen, the subset size used for finding the two images correlated by in the DIC method, the strain smoothing filter size used in the DIC method [21], the noise in the digital image [22], etc., there are many possibilities for further improvements to the O-GFA apparatus.

Apart from the DIC method, an improvement in the accuracy of GFA index can be achieved by the selection of a thin walled cylinder of relatively highly deformable material, for example, aluminum, which has been used in our case. From the cylinder material point of view, another source of error in the experiment and the GFA index's inaccuracy could be the additional friction due to the indentation of a harder material's powder grains into the surface of the softer material of the aluminum cylinder's inner wall. To avoid this, the surface of the aluminum cylinder was polished before the start of our experiment. However, the inspection of the cylinder's inner wall surface with a digital optical microscope has shown the presence of indentation marks of the stainless steel 316 L

powder grains into the polished inner wall surface of the aluminum cylinder. In further experiments, this should be prevented by the selection of the proper material combination of the powder and the cylinder wall.

Furthermore, increasing the diameter of the thin-walled cylinder would additionally contribute to a decrease of the influence of the wall friction on the calculated GFA index, and as motioned above the standardisation of the integration length and the related length of the cylinder, and the granular material's particle and the cylinder diameter ratio, would contribute to a better comparison and a better physical interpretation of the GFA index values in the future, which would make the O-GFA apparatus a promising tool for a granular material's GFA index calculation and the related internal friction characterization.

## Conclusions

To characterise uniaxially pressure-loaded granular materials and the related internal friction a GFA index can be used. In the paper a novel Optical Granular Friction Analyzer (O-GFA) apparatus using a digital camera and digital image correlation (DIC) method to estimate the GFA index has been presented. To estimate the GFA index a granular material contained in a cylinder is uniaxially loaded by applying a compression force. The related tangential and axial deformations of the cylinder are measured using a DIC method. From the DIC-measured deformations and the related strains on the outer wall, along the axial direction of the cylinder a decrease of the internal vertical  $P_V$  in the axial direction of the cylinder is calculated. On the basis of the vertical internal pressure  $P_V$ , along the axis of the cylinder a GFA index was calculated.

The capabilities of the O-GFA and the DIC method to calculate the GFA index were demonstrated experimentally on three samples of stainless-steel 316 L granular materials with different mean particle sizes  $m = 69 \mu\text{m}$ ,  $105 \mu\text{m}$  and  $130 \mu\text{m}$ . Apart from the simplicity of the proposed method, the results obtained with the O-GFA analyser were also in

good agreement with the results from the literature [2]. By means of the parametric error-analysis method, it was shown that based on the strains measured by the DIC method the vertical internal pressure  $P_V$  that is directly related to the GFA index can be obtained within a 7.54% error.

Besides the relatively low error in the calculation of the vertical internal pressure  $P_V$  and the related higher accuracy of the GFA index, the advantages of the DIC method are the ability to determine the location of the piston–powder contact point and the edge-affected regions, the determination of the integration length  $L$  based on the piston–powder contact point and the resolution of the DIC method, a larger number of measurement points and the fact that the points closer to the piston can be used to calculate the GFA index, which all results in a higher accuracy of the GFA index. The analysis of the results showed that the GFA index nonlinearly depends, i.e., exponential and quadratic like, on the number of points and the distance of the first measurement point from the piston. In the presented case the maximum observed variations of the GFA index with respect to the number of points and the distance of the first measurement point from the piston were 2% and 1.3%, which indicates that the GFA index is relatively robust with respect to these two parameters.

Additionally, an analytical relation between Janssen's parameters i.e. the internal pressure ratio  $K_{av}$  and internal friction  $\mu_{av}$ , and the GFA index, similar to the expression developed by Schulze et al. [13], was experimentally confirmed. The later suggests that the GFA index alone can be used to characterize the flowability of a granular material instead of measuring the individual properties, including the internal friction and the lateral pressure ratio of the granular material.

**Acknowledgements** Authors acknowledge the financial support of the Slovenian Research Agency (research core funding No. P2 - 0241).

**Open Access** This article is licensed under a Creative Commons Attribution 4.0 International License, which permits use, sharing, adaptation, distribution and reproduction in any medium or format, as long as you give appropriate credit to the original author(s) and the source, provide a link to the Creative Commons licence, and indicate if changes were made. The images or other third party material in this article are included in the article's Creative Commons licence, unless indicated otherwise in a credit line to the material. If material is not included in the article's Creative Commons licence and your intended use is not permitted by statutory regulation or exceeds the permitted use, you will need to obtain permission directly from the copyright holder. To view a copy of this licence, visit <http://creativecommons.org/licenses/by/4.0/>.

## References

- Schulze D (2007) Powders and bulk solids. Springer-Verlag, Berlin Heidelberg
- Bek M, Gonzalez-Gutierrez J, Moreno Lopez JA et al (2016) Apparatus for measuring friction inside granular materials – granular friction analyzer. Powder Technol 288:255–265. <https://doi.org/10.1016/j.powtec.2015.11.014>
- Chung YC, Lin CK, Chou PH, Hsiau SS (2016) Mechanical behaviour of a granular solid and its contacting deformable structure under uni-axial compression – part I : joint DEM – FEM modelling and experimental validation. Chem Eng Sci 144:404–420. <https://doi.org/10.1016/j.ces.2015.11.024>
- Carson JW, Pittenger BH, Jenike JI (1998) Bulk properties of powders. ASM handbook, Powder Met Technol Appl 7:834–839. <https://doi.org/10.1361/asmhba00015>
- Kato Y, Ohkuma M, Shimada Y, Sunada H (2005) Evaluation of flowability of surface-modified preparations by the measurement of the inter-particle adhesive force. J Drug Dev Sci Tech 15(3): 217–222
- Campbell CS (2006) Granular material flows – an overview. Powder Technol 162:208–229. <https://doi.org/10.1016/j.powtec.2005.12.008>
- Torres-Serra J, Romero E, Rodríguez-Ferran A et al (2017) Flowability of granular materials with industrial applications – an experimental approach. EPJ Web Conf. 140:03068. <https://doi.org/10.1051/epjconf/201714003068>
- Janssen HA (1895) Versuche ueber Getreidedruck in Silonzellen (on the measurement of pressure in grain silos). Zietschrift des Vereines Deutscher Ingenieure 39:1045–1049
- Vlachos N, Chang IT (2011) Investigation of flow properties of metal powders from narrow particle size distribution to polydisperse mixtures through an improved hall-flowmeter. Powder Technol 205:71–80. <https://doi.org/10.1016/j.powtec.2010.08.067>
- Geldart D, Abdullah EC, Hassanpour A et al (2006) Characterization of powder flowability using measurement of angle of repose. China Particuology 4:104–107. [https://doi.org/10.1016/S1672-2515\(07\)60247-4](https://doi.org/10.1016/S1672-2515(07)60247-4)
- Schulze D (1994) Development and application of a novel ring shear tester. Aufbereitungs-technik 35:524–535
- Jenike A (1961) Storage and flow of solids. Eng Exp Stat, Bull No 123. University of Utah, Salt Lake City
- Schulze D (2016) Comment on the paper “Apparatus for measuring friction inside granular materials – Granular friction analyzer”, Marko Bek et al. Powder Technol 288 (2016):255–265 [1]. Powder Technol 301:886–888. <https://doi.org/10.1016/j.powtec.2016.07.024>
- Sadd MH (2014) Elasticity: theory, applications, and numerics, 3rd edn. Academic, Boston
- Khoo S-W, Karuppanan S, Tan C-S (2016) A review of surface deformations and strain measurement using two-dimensional digital image correlation. Metrol Meas Syst 23:461–480
- Blaber J, Adair B, Antoniou A (2015) Ncorr: open-source 2D digital image correlation Matlab software. Exp Mech 55:1105–1122. <https://doi.org/10.1007/s11340-015-0009-1>
- Peters WH, Ranson W (1982) Digital imaging techniques in experimental stress analysis. Opt Eng 21:427–431
- [http://en.wikipedia.org/wiki/6061\\_aluminium\\_alloy](http://en.wikipedia.org/wiki/6061_aluminium_alloy). Accessed 31 Dec 2019
- Marine A (2009) EN AW-6060 – EN AW-Al Mg Si
- Bevington PR, Robinson KD (1992) Data reduction and error analysis for the physical sciences. McGraw-Hill, New York
- Correlated Solutions Application Note AN – 1701 Speckle Pattern Fundamentals
- Baldoni J, Lionello G, Zama F, Cristofolini L (2016) Comparison of different filtering strategies to reduce noise in strain measurement with digital image correlation. J Strain Anal Eng Des 51:416–430. <https://doi.org/10.1177/0309324716646690>

**Publisher's Note** Springer Nature remains neutral with regard to jurisdictional claims in published maps and institutional affiliations.

